

The warm absorber of the Seyfert 1 galaxy H1419+480

X. Barcons*, F.J. Carrera, M.T. Ceballos

Instituto de Física de Cantabria (CSIC-UC), 39005 Santander, Spain

June 2003

ABSTRACT

The bright Seyfert 1 galaxy H1419+480 ($z \sim 0.072$), whose X-ray colours from earlier HEAO-1 and *ROSAT* missions suggested a complex X-ray spectrum, has been observed with *XMM-Newton*. The EPIC spectrum above 2 keV is well fit by a power-law with photon index $\Gamma = 1.84 \pm 0.01$ and an Fe K α line of equivalent width ~ 250 eV. At softer energies, a decrement with respect to this model extending from 0.5 to 1 keV is clearly detected. After trying a number of models, we find that the best fit corresponds to OVII absorption at the emission redshift, plus a 2σ detection of OVIII absorption. A photoionised gas model fit yields $\log \xi \sim 1.15 - 1.30$ (ξ in erg cm s^{-1}) with $N_H \sim 5 \times 10^{21} \text{ cm}^{-2}$ for solar abundances. We find that the ionized absorber was weaker or absent in an earlier *ROSAT* observation. An *IUE* spectrum of this source obtained two decades before shows a variable (within a year) CIV absorber outflowing with a velocity $\sim 1800 \text{ km s}^{-1}$. We show that both X-ray and UV absorptions are consistent with arising in the same gas, with varying ionisation.

Key words: X-rays: galaxies, galaxies: active

1 INTRODUCTION

X-ray spectral studies of radio-quiet Active Galactic Nuclei (AGNs), reveal very frequently the presence of ionised material. This was first noted by Halpern (1984), based on *Einstein* IPC data, where it was also noted that these absorbers vary. Evidence for ionized absorption along the line of sight was provided by Nandra & Pounds (1992), based on the detection of an absorption edge in *ROSAT* observations of the Seyfert 1 galaxy MCG-6-30-15. Fabian et al (1994) were able to disentangle the OVII and OVIII K-edges of this warm absorber using the much better spectral resolution of *ASCA*.

In the years that followed, it became evident that warm absorbers are ubiquitous among Seyfert 1 galaxies. Reynolds (1997) and George et al (1998) showed that more than 50% of Seyfert 1s contain a warm absorber. These are produced by partially ionised gas with total column density in the range $N_H \sim 10^{21} - 10^{23} \text{ cm}^{-2}$, probably located at or outside the Broad Line Region (Reynolds & Fabian 1995).

With the advent of higher resolution grating spectrographs on board *Chandra* and *XMM-Newton* much more detailed studies of ionized absorbers have become possible. X-ray spectra obtained with the Reflection Grating Spectrograph (den Herder et al 2001) on board *XMM-Newton* have shown that the absorbing gas has often various components with different outflowing velocities and clearly distinct ionisation states (see Sako et al 2001 for IRAS 13349+2438 and

Blustin et al 2002 for NGC 3783). One of the most remarkable features discovered in these spectra is the presence of Unresolved Transition Arrays (UTAs) of Fe M lines, which could mimic the shape of absorption edges when observed at the lower spectral resolution typical of CCDs.

Detailed studies of particular AGN which exhibit X-ray ionized absorption features also demonstrate that there is frequently a narrow-line absorber related to the AGN (i.e. an *associated* absorber) in the ultraviolet band, normally showing up as a CIV $\lambda\lambda 1548, 1550$ absorption feature (Mathur 1994, Mathur et al 1994, Mathur, Elvis & Wilkes 1995). The same photoionized outflowing gas can provide the UV absorption lines and the ionized absorption features seen in X-ray spectra. More recently, Crenshaw et al (1999) found in a systematic study of UV absorption lines towards nearby radio-quiet AGN, that *all* objects showing UV associated absorption systems have a corresponding warm absorber in the X-rays.

Variability has also been found in some of these warm absorbers. Fabian et al (1994) reported different absorption optical depths in the best-studied warm absorber towards MCG-6-30-15. Later, Otani et al (1996) showed, using a 4-day long *ASCA* observation of this particular Seyfert 1, that the OVIII K edge (at a rest frame energy of 0.871 keV) varied on scales of ~ 10 ks, while the OVII K-edge (at a rest frame energy of 0.739 keV) remained constant. Otani et al (1996) interpreted this in terms of two different ionized absorbers, a high ionisation (OVIII) absorber located within the BLR and a lower ionisation absorber (OVII) probably associated to the Narrow Line Region (NLR).

* E-mail: barcons@ifca.unican.es

H1419+480 was discovered in the Modulation Collimator - Large Area Sky Survey (MC-LASS) conducted with the HEAO-1 observatory (Wood et al 1984). The inferred 2-10 keV flux was $\sim 2 \times 10^{-11}$ erg cm $^{-2}$ s $^{-1}$, assuming a power law spectrum with a canonical $\Gamma = 1.7$ (Ceballos & Barcons 1996). Although the modulation collimator helped to pin down the position of the X-ray source, the flux could be severely affected by the contribution of unresolved sources within the collimator field of view. The *ROSAT* All-Sky Survey (RASS) also detected this source (see Schwobe et al 2000), with a 0.5-2 keV flux (corrected for Galactic absorption) of $\sim 7 \times 10^{-12}$ erg cm $^{-2}$ s $^{-1}$ and an additional PSPC pointed observation conducted in 1992 found a flux of $\sim 3 \times 10^{-12}$ erg cm $^{-2}$ s $^{-1}$. In both cases the PSPC hardness ratio was ~ 0 which excluded a significant photoelectric absorption by cold gas.

Remillard et al (1993) identified H1419+480 with a broad-line type 1 AGN at $z = 0.072$ ($RA = 14^h 21^m 29.60^s$, $DEC = +47^\circ 47' 27''$). Appendix A presents our own optical spectroscopic observations of H1419+480, which confirm that this source is a broad-line AGN with $z = 0.07229$, as derived from the [OIII] emission doublet.

Ceballos & Barcons (1996) analyzed a sample of sources detected both in the MC-LASS sample and by *ROSAT* (which included H1419+480). The large decrement of the flux from hard to soft X-rays is suggestive of heavy photoelectric absorption, which is at odds with the value reported for the PSPC hardness ratio. This was interpreted by Ceballos & Barcons (1996) as evidence for complex absorption, that could be modelled either in terms of an ionized absorber or in terms of a partial covering cold absorber.

In this paper we present *XMM-Newton* EPIC observations of H1419+480. We find that the source has changed the soft X-ray flux again and that its 2-10 keV flux is almost a factor 3 lower than the HEAO-1 one. A warm absorber is unambiguously seen in the *XMM-Newton* data, through mostly OVII absorption, but we argue that this warm absorber was weaker or absent in the previous pointed *ROSAT* observation. An associated CIV absorption line is seen in an *International Ultraviolet Explorer (IUE)* spectrum of this source taken more than 20 years ago, but it is not seen in a similar observation taken one year later. We find that both X-ray and UV absorption can be explained in terms of the same amount of gas but varying ionising conditions.

2 X-RAY PROPERTIES

2.1 *XMM-Newton* observations

H1419+480 was observed by *XMM-Newton* (Jansen et al 2001) for 27 ks on the 27th of May of 2002, during revolution 451 (obsid=0094740201), as part of the Guaranteed Time programme of the Survey Science Centre. In this paper we analyze only the data obtained by the EPIC MOS (Turner et al 2001) and EPIC pn (Strüder et al 2001) cameras. The source is clearly detected by the RGS spectrographs, but it is far too faint to deliver any scientifically interesting results. The OM (Mason et al 2001) was used to obtain images in the filters U, B and UVW1.

All 3 EPIC cameras had the 'Thin 1' filter on, and they were operated in partial window mode (MOS1 and MOS2)

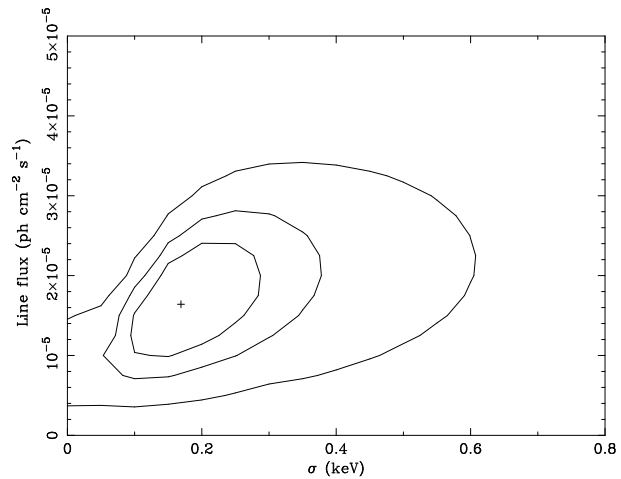


Figure 1. Confidence contours (1,2 and 3 sigma) for the flux versus dispersion of the Fe line

and small window mode (pn). Exposure times (excluding overheads) were 13 ks for the MOS cameras and 20 ks for the pn camera. However, most of the exposure time was lost due to high background flaring. After cleaning out these intervals, good-time intervals of ~ 8 ks were left for the MOS1 and MOS2 detectors, and 3 ks were left for the pn detector. Fortunately H1419+480 is bright enough (5 cts/s in the EPIC pn camera) to provide a large enough number of counts for spectral analysis.

Event files for the 3 EPIC detectors were taken from the distributed pipeline products, which were obtained by processing the observation data file with SAS v5.3.3. We filtered out high-background intervals, keeping only the most reliable single and double events and, in the case of EPIC pn, by removing those with low spectral quality. Calibration matrices were generated by using SAS v5.4.1, which we found to solve some problems at energies 0.5-1 keV with respect to the SAS v5.3.3 calibration.

X-ray spectra for H1419+480 and background, were extracted from the 3 EPIC cameras. The background spectrum was extracted from regions in the same chip as the source but not illuminated by H1419+480. This was also done in the MOS data, as opposed to source-free regions in the outer chips, to prevent vignetting affecting the background subtraction. The source plus background pn, MOS1 and MOS2 spectra were binned individually into bins containing at least 20 counts each. To fit spectral models to these data, `xspec` version 11.2.0 was used (Arnaud 1996). Bins outside the 0.2-12 keV bandpass were ignored. At the time of performing this analysis, a calibration problem (probably produced for an incorrect redistribution matrix) of the MOS detectors below 0.5 has been reported. In this paper we have taken the conservative approach of ignoring all MOS data below 0.5 keV.

2.2 The 2-12 keV X-ray spectrum

We first fit the 2-12 keV spectrum to determine the underlying continuum. A single power law fit gave $\chi^2 = 305.96$ for 311 degrees of freedom (two parameters fitted), but with obvious residuals around 6 keV. Adding a redshifted gaussian emission line improved the fit substantially to $\chi^2 = 290.17$

Table 1. X-ray spectral parameters of H1419+480 for the 2-12 keV fit. All errors are 90% confidence for 1 interesting parameter.

Parameter	Value	Units
zgauss	($z = 0.07229$)	
E_{line}	$6.52^{+0.12}_{-0.11}$	keV
σ_{line}	$0.17^{+0.14}_{-0.06}$	keV
F_{line}	$(1.7^{+0.8}_{-0.8}) \times 10^{-5}$	ph cm ⁻² s ⁻¹
zopwerlaw	($z = 0.07229$)	
Γ	$1.84^{+0.02}_{-0.01}$	
A_{Γ}	$(2.53 \pm 0.03) \times 10^{-3}$	ph cm ⁻² s ⁻¹ keV ⁻¹

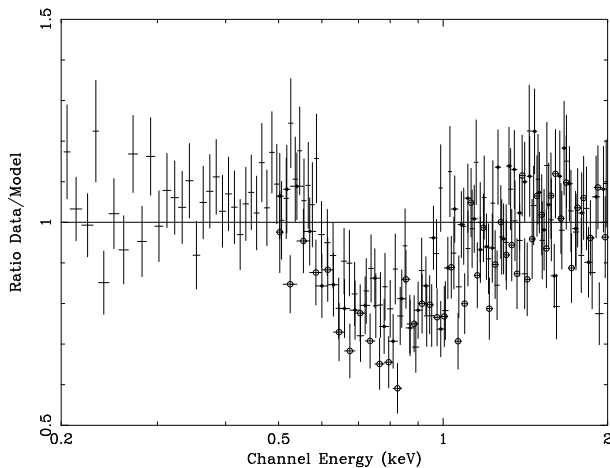


Figure 2. XMM-Newton EPIC spectral ratio of data to a power law plus galactic absorption model, where the 0.5-1 keV region has been excluded from the fit. Crosses are from EPIC pn, filled circles from EPIC MOS1 and hollow circles from EPIC MOS2. The data points have been binned into 100 count bins for illustration purposes only.

for 308 degrees of freedom. The F-test assigned a significance to the detection of this line of 99.90%. Parameters resulting from the fit are listed in table 1, while Fig. 1 shows the confidence contours in the line flux versus line dispersion parameter space. The line equivalent width derived from these parameters is 240^{+125}_{-110} eV. All parameters are entirely consistent with those from other Seyfert 1 galaxies (Nandra & Pounds 1994). The EPIC pn spectrum shows a hint of a residual towards low energies, reminiscent of relativistic effects in a disk line, but since the MOS1 and MOS2 spectra do not show such residuals we do not explore this point any further. This emphasizes again the importance of calibration in the detection of weak features (such as relativistic line profiles) in moderate signal-to-noise data. In what follows the energy of the Fe line and its width have been fixed to their best-fit values (see Tab. 1) in order to prevent runaway solutions with unphysical parameters (e.g., extremely broad lines).

2.3 The 0.2-2 keV X-ray spectrum

We then extend the fit to 0.2 keV, including photoelectric absorption from the Galaxy ($N_H = 1.65 \times 10^{20}$ cm⁻²). The fit is not good, with $\chi^2 = 1140.45$ for 795 degrees of free-

dom. There are obvious negative residuals as shown in fig. 2, where the 0.5-1 keV band has been excluded from the fitting region. We have explored a number of model fits in trying to understand this feature.

2.3.1 Absorption plus soft excess

We first try to fit the spectrum with an absorbed power law plus a soft excess in trying to mimic the negative feature seen in the residuals. The soft excess is modelled as a steep power law (a black body model did not converge to a better value of the χ^2). The best fit yields a minimal reduced $\chi^2_{\nu} = 936.03/792$, corresponding to a $\Gamma_{\text{soft}} = 2.40 \pm 0.09$ and to an intrinsic absorption (at the redshift of the Seyfert 1 $z = 0.07229$) of $N_H = (5.7^{+1.2}_{-1.0}) \times 10^{21}$ cm⁻². Although the improvement in the χ^2 is very significant, strongly correlated negative residuals in the 0.5-1 keV band persist. One of the models suggested by Ceballos & Barcons (1996) to explain the unusual X-ray colours of this source on the basis of a partial covering cold absorber, yields an even worst $\chi^2 = 983.78$.

2.3.2 Single ion absorption

The absorption trough seen in the residuals is clearly reminiscent of an absorption edge or a UTA. The “equivalent width” of the absorption feature seen in the data is ~ 0.7 Å, which is twice larger than the values typically found in the Fe M UTAs. Besides, the absorption feature in H1419+480 spreads over ~ 5 Å, while the Fe M UTAs spread over 1.5 Å in the RGS. The spectral resolution of EPIC at the energies of interest is 0.6 – 1 Å, and therefore would be unable to spread a UTA up to 5 Å. A further argument against the bulk of this feature being due to a Fe M UTA comes from the fit to a multi-ion photoionised absorber (see subsection 2.3.3) where all Fe M lines are included and yet the absorber’s parameters are very similar to those fitted by assigning the feature to (mostly) the OVII absorption edge. Therefore we conclude that, although UTAs can contribute to the detected absorption feature, they cannot account for all of it. We therefore start by attempting to interpret the negative spectral feature in terms of an absorption edge.

Indeed, adding a single absorption redshifted edge to the data results in a minimal $\chi^2_{\nu} = 854.11/793$ (i.e., substantially better than the soft excess model). The edge energy is $E_{edge} = 715^{+10}_{-19}$ eV with a maximum depth of $\tau_{edge} = 0.58^{+0.07}_{-0.05}$. If interpreted as an intrinsic OVII absorption K-edge, at a rest frame energy of 739 eV, the absorber should be infalling towards H1419+480 at a velocity $v = 9100^{+7200}_{-3800}$ km s⁻¹. This velocity shift is significantly larger than the velocity outflow found in the best studied cases with the X-ray gratings.

One fact that might contribute, at least partly, to this shift is the presence of resonance absorption lines from the same ion, which are unresolved by EPIC, but still contributing to the shape of the absorption feature. This fact has been noted, among others, by Lee et al (2001) in the analysis of the *Chandra* data of the Seyfert 1 galaxy MCG-6-30-15. We therefore prefer to model the single ion absorption by the **siabs** model released in the PHOTOION package (Kinkhabwala et al 2003), under the assumption

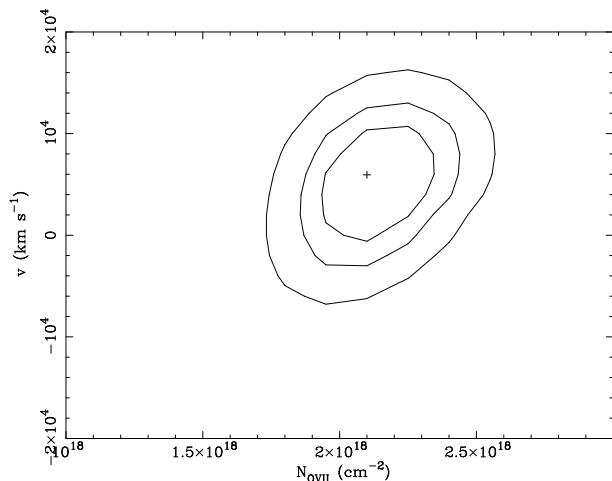


Figure 3. Best fit and confidence contours (1,2, and 3 sigma) for the parameters in the single ion absorption model *xiabs* to the absorption feature.

that the feature corresponds to OVII. The fit results in a $\chi^2_\nu = 851.41/793$ corresponding to a column density $N_{OVII} = (2.1 \pm 0.3) \times 10^{18} \text{ cm}^{-2}$ and an infall velocity of $v = 6000^{+5400}_{-7350}$ towards the source. Fig. 3 shows the confidence contours for these two parameters. We note that the fit is even marginally better than the one provided by the K-edge solely and that the velocity shift is now much more moderate (and consistent with zero), as in better-studied warm absorbers.

2.3.3 Multiple-ion absorption

Although the single ion absorption fit does not leave obvious residuals in the X-ray data, we have attempted to add an OVIII absorber with the same recession velocity than the OVII absorber fixed at the best fit value of 6000 km s^{-1} . The χ^2_ν further decreases to $846.68/792$ by just adding one parameter (the OVIII column density). The F-test statistic yields a significance of only 96.4% for this new component. Fig 4 shows the confidence contours in the OVII and OVIII column density parameter space. Fig. 5 shows the EPIC spectrum together with the 2 single ion absorption spectral fit, along with the featureless residuals.

We have also explored the possibility of describing the absorption feature in terms of a solar abundance photoionized gas, by using the model *xiabs* from the PHOTOION package (Kinkhabwala et al 2003). The best fit, by fixing the infall velocity at 6000 km s^{-1} , is reached for $\log \xi = 1.30 \pm 0.1$ and a total H column density of $N_H \sim (5.1 \pm 0.7) \times 10^{21} \text{ cm}^{-2}$ with a $\chi^2_\nu = 871.32/793$. Contour plots are shown in Fig. 6. However the fit is not as good as that for the OVII and OVIII absorption only, presumably due to unmatched features from other elements.

The *xiabs* model used does not include thermal (collisional) ionisation in the absorbing gas. We illustrate the effects of collisional ionisation by computing the values of N_{OVII} and N_{OVIII} for a photoionised gas at a temperature $T = 3 \times 10^5 \text{ K}$ (typical of warm absorber models) and assuming a gas density of 10^{10} cm^{-3} (e.g., as in the Mathur et al 1994 models), although this last parameter is only marginally relevant as the gas is optically thin. We have used

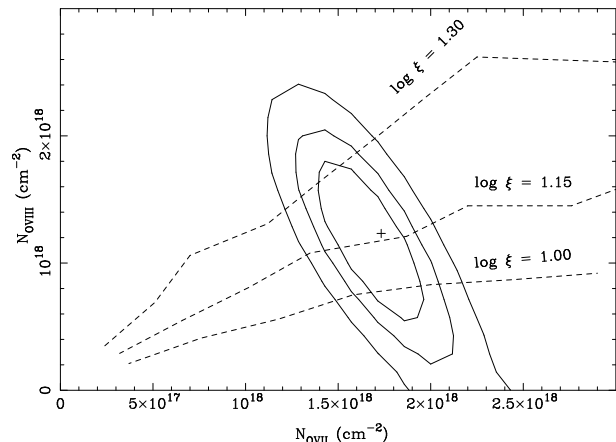


Figure 4. Best fit and confidence contours (1,2, and 3 sigma) for the OVII and OVIII column densities by fitting 2 single ion absorption with infall velocity fixed at 6000 km s^{-1} . The dashed lines show the predictions for a thermal ($T = 3 \times 10^5 \text{ K}$) photoionised gas and representative values of the ionisation parameter ξ , for a range of H column densities.

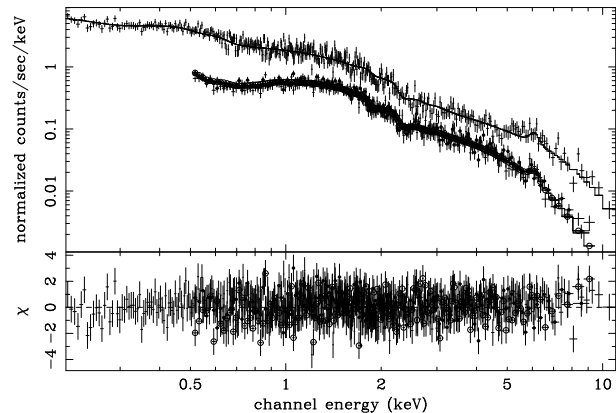


Figure 5. *XMM-Newton* EPIC spectrum and residuals with respect to the best-fit model consisting in a power law plus Fe line and absorption for both OVII and OVIII. Crosses are from EPIC pn, filled circles from EPIC MOS1 and hollow circles from EPIC MOS2.

XSTAR (version 2.1) along with solar abundances and the results are shown in Fig. 4 for a few values of the ionisation parameter. In this case, some of the ionisation takes place by collisions and therefore the required ionisation parameter is marginally smaller ($\log \xi \sim 1.15$). The required value for the column density is also around $N_H \sim 5 \times 10^{21} \text{ cm}^{-2}$. With this we conclude that both the ionisation parameter and the amount of gas along the line of sight are fairly well established.

2.4 Variability

Although the *XMM-Newton* exposure is relatively short, we have also explored whether the source varied within the observation. Counts have been accumulated in the 0.5-2 keV and 2-12 keV band. The reason for this resides in the fact that the 0.5-2 keV band is dominated mostly by the absorbed component and the 2-12 keV by the underlying continuum (plus Fe line).

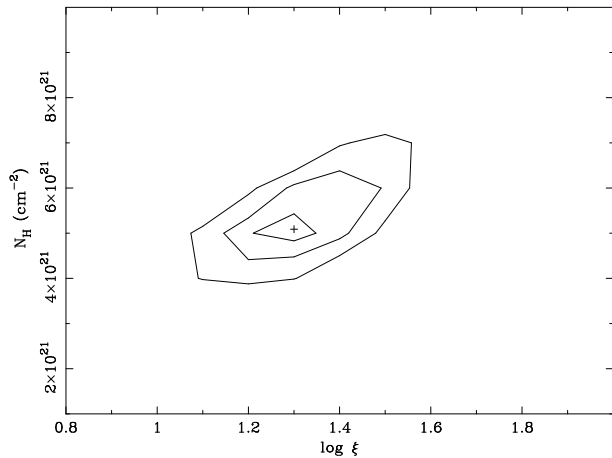


Figure 6. Best fit and confidence contours (1, 2, and 3 sigma) for the total column density and ionisation parameter ξ (in units of erg cm s^{-1}) after fitting the X-ray spectrum to a photoionised gas with solar abundances (model *xiaabs*)

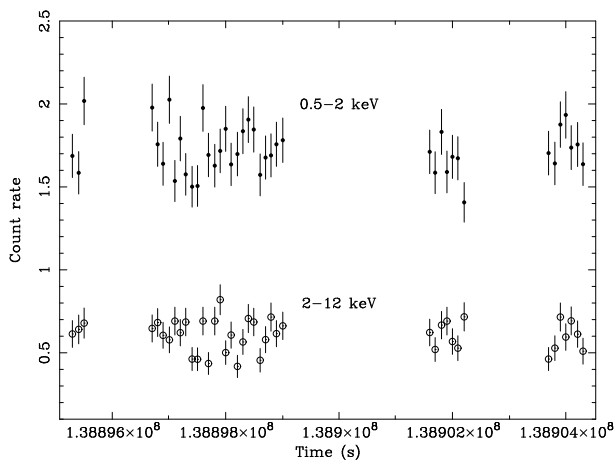


Figure 7. EPIC-pn light curves of H1419+480 in the 0.5-2 keV and 2-12 keV bands. The gaps are due to high-background flaring intervals.

Counts have been grouped into 100 s bins, which produced an EPIC pn count rate of 1.7 ct/s in the 0.5-2 keV band and 0.6 ct/s in the 2-12 keV band. Although it is a minor correction, the lightcurve of the background has been scaled and subtracted from the source’s lightcurve. Fig. 7 shows the resulting lightcurves of H1419+480. In order to look for the significance of any variability, we fit a constant value to every lightcurve and compute the minimum χ^2 . For the 0.5-2 keV band, $\chi^2 = 48.58$ for 41 points, which yields a probability of the source being variable of only 83%. In the 2-12 keV band $\chi^2 = 60.9$, with a probability of the source being variable of 98%. We have further checked whether any marginal variations are different in both bands, by fitting a constant to the difference between the 2-12 keV and 0.5-2 keV count rates. The χ^2 fit to a constant yields $\chi^2 = 32.0$ for 40 points, which is entirely consistent with no X-ray colour variations. We therefore conclude that there is no significant variability of the source within the *XMM-Newton* observation and that in any case variations preserve the X-ray colours of the source. Therefore there are no constraints on the physical models for this source derived from variability.

2.5 Comparison to previous X-ray observations

Using the best-fit model with two single ion absorption (OVII and OVIII), we compute the flux of H1419+480, corrected for Galactic absorption, to be $4.5 \times 10^{-12} \text{ erg cm}^{-2} \text{ s}^{-1}$ in the 0.5-2 keV band and $7.3 \times 10^{-12} \text{ erg cm}^{-2} \text{ s}^{-1}$ in the 2-10 keV band. Adopting currently fashionable cosmological parameters ($H_0 = 70 \text{ km s}^{-1} \text{ Mpc}^{-1}$, $\Omega_m = 0.3$ and $\Omega_\Lambda = 0.7$), the luminosity of H1419+480 is $5.7 \times 10^{43} \text{ erg s}^{-1}$ in the 0.5-2 keV band and $9.2 \times 10^{43} \text{ erg s}^{-1}$ in the 2-10 keV band.

The *XMM-Newton* 2-10 keV flux is almost a factor of 3 smaller than the HEAO-1 flux, a fact that can be at least in part explained by source confusion in the HEAO-1 collimators (see Barcons et al 2003 for a discussion on a similar situation for another source).

There are two *ROSAT* observations of H1419+480 recorded from this source: one from the *RASS* (reported in Schwobe et al 2000) and a second one performed on January 1992 (observation sequence ROR700038), used in Barcons & Ceballos (1996). Table 2 lists some data of these observations, along with expectations from the *XMM-Newton* observation. We have folded our best-fit model to the *XMM-Newton* data through the *ROSAT* PSPC-B response to compute the expected spectral shape in the *ROSAT* observations and to convert count rates to fluxes.

The first obvious conclusion is that the 0.5-2 keV flux has changed significantly between the 3 different observations. The expected spectral shape in the *ROSAT* observations appears similar (but not identical) to the measured one. The PSPC Hardness and Softness Ratios (see caption of table 2 for definitions) expected in the *ROSAT* data from our best-fit model to the *XMM-Newton* spectrum have been computed with and without the OVII and OVIII absorption components. In particular the value measured for SR_1 in the 1992 observation appears consistent with the absence (or weakening) of the absorption features, but largely inconsistent with the presence of the absorption features. We conclude that the absorption features were much weaker or absent during the *ROSAT* observation of H1419+480 in 1992.

3 AN ASSOCIATED CIV ABSORBER

The compelling evidence that X-ray warm absorbers share a common origin with associated narrow-line absorbers in the UV (Crenshaw et al 1999) urged us to search in available archives for UV spectroscopic observations of H1419+480. Unfortunately the *Hubble Space Telescope* (*HST*) has not observed this object with any of the UV spectrographs, but the *IUE* did observe it several times. Table 3 lists the observations conducted with the SWP short wavelength camera (operated at low dispersion $\sim 6 \text{ \AA}$), which encompass both the Ly α $\lambda 1216$ and the CIV $\lambda 1549$ emission lines. We analyzed the INES (*IUE* Newly Extracted Spectra) data from both of these observations.

Fig. 8 shows the spectra obtained by *IUE* during both observations, around the CIV emission line. Only channels which have not been flagged for any reason are plotted. The overall flux shift between both spectra could be either true variability or a calibration problem. The most obvious discrepancy between both spectra occurs at around $\lambda \sim 1651 \text{ \AA}$,

Table 2. Details of *ROSAT* observations of H1419+480, along with expected values of the PSPC Hardness Ratio and Softness ratios derived from the best-fit to the *XMM-Newton* data with and without the OVII+OVIII absorption.

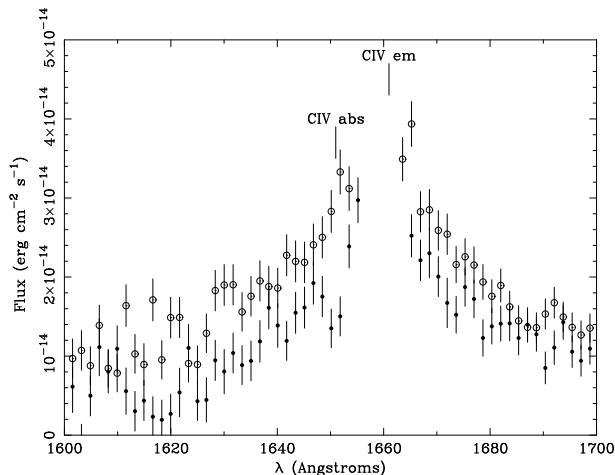
Parameter	<i>ROSAT</i> (RASS)	<i>ROSAT</i> (ROR700038)	<i>XMM-Newton</i> (with absorption)	<i>XMM-Newton</i> (without absorption)
Exposure time (s)	375	1266		
Flux ^a	7×10^{-12}	3×10^{-12}	4.5×10^{-12}	4.5×10^{-12}
<i>HR</i> ^b	$+0.0 \pm 0.1$	-	+0.0	+0.1
<i>SR</i> ₁ ^c	-	$+1.6 \pm 0.2$	+2.4	+1.7
<i>SR</i> ₂ ^d	-	$+0.7 \pm 0.1$	+0.6	+0.7

^a Flux in the 0.5-2 keV band in units of $\text{erg cm}^{-2} \text{s}^{-1}$, corrected for Galactic absorption using the best fit model from table 1

^b PSPC Hardness Ratio $HR = (H - S)/(H + S)$ where S and H are the counts detected in PSPC channels 11-39 and 50-200 respectively.

^c PSPC softness ratio $SR_1 = S_1/H_1$, where S_1 and H_1 are the counts detected in PSPC channels 11-39 and 40-85 respectively.

^d PSPC softness ratio $SR_2 = H_1/H_2$, where H_2 are the counts detected in PSPC channels 86-200.

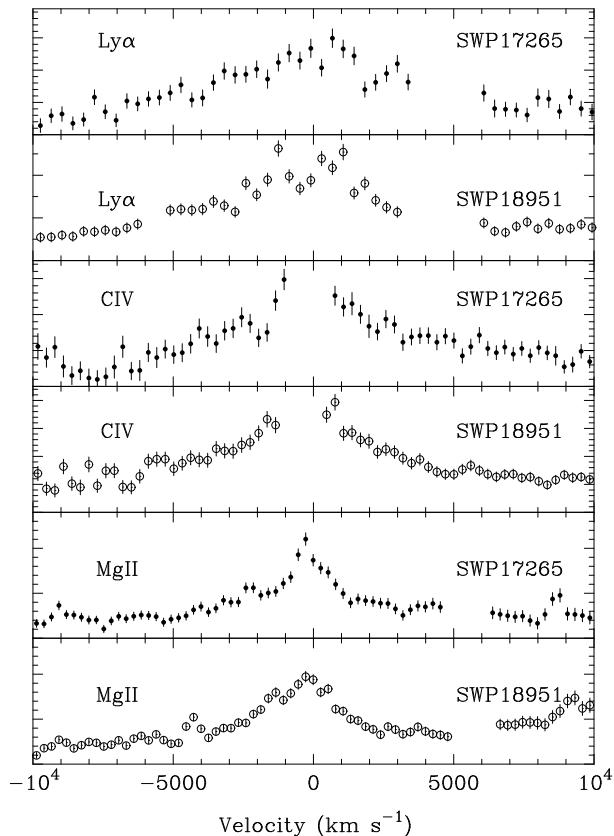
**Figure 8.** *IUE/SWP* spectra of H1419+480 around the CIV emission line. Only datapoints which have not been flagged by any reason are plotted. Filled (hollow) circles are from the SWP17265 (SWP18951) observations respectively.

where the earlier observation (SWP17265) shows a dip that could be an absorption line.

To further investigate this, and keeping in mind that detecting absorption lines on top of emission lines is a difficult task, we have taken the 8 channels ranging from 1643 to 1656 Å in the SWP17265 spectrum. A linear function was fitted to that range, resulting in a $\chi^2 = 17.65$ for 6 degrees of freedom. Multiplying by a gaussian absorption line and freezing its width to the resolution of the spectrograph (i.e., searching for an unresolved line) the χ^2 improved to $\chi^2 = 0.99$ for 4 degrees of freedom. The F-test significance of that feature is 99.7% ($\sim 3\sigma$). The central wavelength is $\lambda_{abs} = 1651.1 \pm 0.5 \text{Å}$, corresponding to an outflowing velocity of $\sim 1800 \pm 90 \text{km s}^{-1}$. The equivalent width is also very uncertain, due to the poor sampling, but formally the best fit is $3_{-0.9}^{+0.7} \text{Å}$.

We have also explored the wings of the Ly α $\lambda 1216$ and MgII $\lambda 2800$ (see fig. 9), but no other obvious absorption lines are evident. We conservatively estimate that a 3σ upper limit for any Ly α absorption line present in this spectrum is about 3Å .

At the 6Å resolution of this setup, the CIV doublet ($\lambda\lambda 1548, 1550$) is unresolved and, obviously, we cannot measure directly the absorbing column density. Fig 10 shows

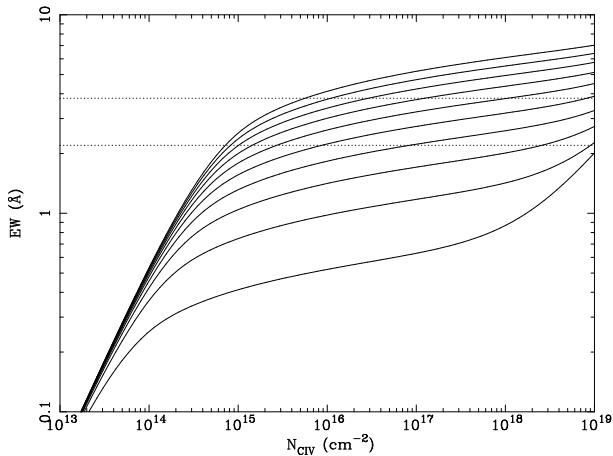
**Figure 9.** *IUE/SWP* velocity spectra of H1419+480 around the Ly α , CIV and MgII emission lines. Only datapoints which have not been flagged by any reason are plotted. Filled (hollow) circles are from the SWP17265 (SWP18951) observations respectively.

the curve of growth (i.e., equivalent width versus column density) for the whole CIV doublet and a range of velocity dispersion parameters. As usual a Voigt profile has been assumed for each line in the doublet, with velocity width parameter $b = \sqrt{2}\sigma$ (σ is the velocity dispersion of the gas, assumed Maxwellian), damping constant $2.64 \times 10^8 \text{s}^{-1}$ and a *total* oscillator strength of 0.28 (which is the sum of the oscillator strengths for the two lines). The approximation introduced by Whiting (1968) to the Voigt profile (accurate to better than 5%) has been used.

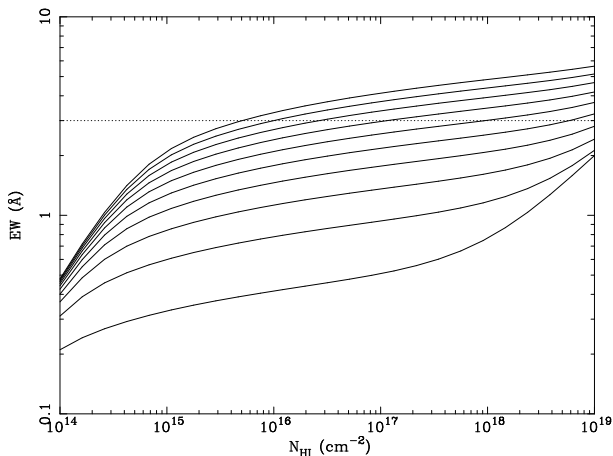
The amount of CIV absorbing gas is very uncertain,

Table 3. Details of *IUE*/*SWP* observations of H1419+480.

Image identification	Date	Exposure (s)
SWP17265	1982-06-19	8400
SWP18951	1983-01-05	9000


Figure 10. Curve of growth for the CIV $\lambda\lambda 1548,1550$ doublet (continuous lines). Velocity dispersion parameters $b = \sqrt{2}\sigma$ (σ is the velocity dispersion of the gas) range from 20 to 200 km s^{-1} in steps of 20 km s^{-1} from bottom to top. The dotted lines show the measured equivalent width formal 90% confidence interval.

as the measured equivalent width falls in the saturated part of the curve of growth, but values around $N_{CIV} \sim 10^{15-16} \text{ cm}^{-2}$ would be appropriate for Doppler velocity parameters around 100 km s^{-1} . In Fig. 11 we also plot the curve of growth for HI Ly α , using an oscillator strength of 0.416 and a damping constant of $4.7 \times 10^8 \text{ s}^{-1}$, along with the upper limit of 3 \AA . We can see that relatively large HI column densities (up to $10^{17-18} \text{ cm}^{-2}$) could go undetected for similar values of the Doppler velocity parameter.


Figure 11. Curve of growth for the HI Ly α $\lambda 1216$ transition (continuous lines). Velocity dispersion parameters as in Fig. 10. The dotted line shows the adopted 3σ upper limit for the detection of this line in the *IUE* spectra.

4 DISCUSSION

Establishing a link between the X-ray and the UV absorbing gas is difficult in this case, as the observations are not simultaneous. We can, however, test whether or not it is plausible that the same or a similar amount of gas (perhaps in a different ionisation state) produced both absorption features.

The X-ray absorbing gas has a fairly well determined column of $N_H \sim 5 \times 10^{21} \text{ cm}^{-2}$ and it is highly ionized ($\log \xi \sim 1.1 - 1.3$). Its velocity with respect to the emission redshift is only poorly defined by the EPIC data but consistent with zero. The absorber was significantly weaker or absent in the 1992 *ROSAT* observation.

The UV gas detected as a CIV associated absorber in the 1982 *IUE* observation of H1419+480, has a fairly well determined outflowing velocity of $1800 \pm 90 \text{ km s}^{-1}$, but its CIV column density is only poorly constrained $\sim 10^{15} N_{15} \text{ cm}^{-2}$ with $N_{15} \sim 1 - 10$. No HI Ly α or MgII absorption are found, although the *IUE* spectra at the Ly α region are noisier than around the CIV and MgII lines. The total column density implied by the CIV absorption is

$$N_H = 2.4 \times 10^{18} N_{15} f_{CIV}^{-1} \text{ cm}^{-2} \quad (1)$$

where f_{CIV} is the fraction of C which is in CIV ionisation state. Indeed this is a completely unknown parameter, as we cannot determine the ionisation parameter of this gas which applies to the 1982 observation from a single UV unresolved absorption feature. We must restrict ourselves to check whether a value of $N_H \sim 5 \times 10^{21} \text{ cm}^{-2}$, as in the X-ray absorber, can be obtained for reasonable ionisation conditions.

Using XSTAR (version 2.1) we have computed ionization fractions for CIV (f_{CIV}), HI (f_{HI}) and MgII (f_{MgII}) for a range of values of $\log \xi \sim 1 - 1.5$, assuming the gas temperature fixed at $T = 3 \times 10^5 \text{ K}$ and with a spectral shape given by a $\Gamma = 1.84$ power law. As pointed out by, e.g., Mathur et al (1994) this might result in a very inaccurate shape of the UV ionizing continuum and instead a more accurate shape should be used. However, for the purposes of this illustrative exercise, where the ionising parameter is essentially unknown, this rough modelling of the ionising spectrum is good enough.

For this range of parameters, f_{CIV} (f_{HI}) decreases from 7.1×10^{-3} (3.4×10^{-5}) for $\log \xi = 1.0$ to 4.4×10^{-5} (4.0×10^{-6}) for $\log \xi = 1.5$. f_{MgII} is zero for this range of ionisation. If we adopt the amount of gas seen in the X-ray absorber ($N_H \sim 5 \times 10^{21} \text{ cm}^{-2}$), HI Ly α would be difficult to detect in all the explored range of ionisations, as the HI column density would be below 10^{17} cm^{-2} . However, N_{CIV} would range from $1.6 \times 10^{16} \text{ cm}^{-2}$ for the lower ionisation states explored down to $\sim 10^{14} \text{ cm}^{-2}$ in the opposite extreme. In conclusion, there is a range of ionisation parameters, in fact with values around those measured from the X-ray absorber ($\log \xi \sim 1.3$), where it is plausible to observe the CIV absorption line and no HI Ly α or MgII absorptions. A slightly higher ionisation brings also the CIV absorption below detection limits.

5 CONCLUSIONS

The bright Seyfert 1 galaxy H1419+480 has been shown to be variable in X-rays by comparing our *XMM-Newton* ob-

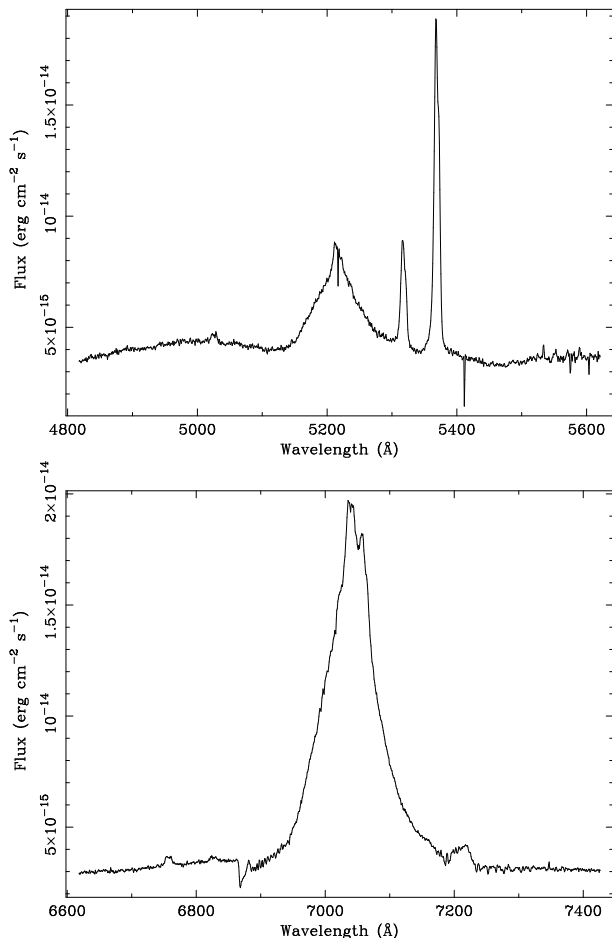


Figure 12. Optical spectrum of H1419+480.

servations with earlier *ROSAT* data. A warm absorber is clearly seen mostly through OVII absorption, but also with $\sim 2\sigma$ evidence for OVIII absorption, in the *XMM-Newton* data at the emission redshift. The absorber was weaker or absent in a *ROSAT* pointed observation performed in 1992. The absorber contains a gas column of $N_H \sim 5 \times 10^{21} \text{ cm}^{-2}$, and the ionisation parameter is around $\log \xi \sim 1.15 - 1.3$ depending on whether or not ionisation by collisions is included.

An *IUE* observation of H1419+480 conducted in 1982 shows $\sim 3\sigma$ detection for a CIV associated absorber, outflowing with a velocity $\sim 1800 \pm 90 \text{ km s}^{-1}$. This confirms the close link between X-ray ionized absorbers and UV associated absorption reported, among others, by Crenshaw et al (1999). This absorption line was not present in an *IUE* observation obtained roughly 1 year later.

We find that a plausible common origin for all these variable absorption phenomena can be understood in terms of the same (or similar) amount of photoionised gas, but with varying ionisation state. Indeed, for values of the ionisation parameter similar to those inferred from the X-ray observations, we find that the X-ray absorbing gas could have produced the CIV absorption feature without any detectable HI Ly α or MgII lines. A slightly higher ionisation would explain the lack of the CIV absorption feature in the *IUE* observation in 1983.

We therefore conclude that H1419+480 has a variable

ionised absorber. Both X-ray and associated UV absorbers are detected at different epochs in this object, along the lines of the sample studied by Crenshaw et al. (1999). Furthermore, we have shown that both absorbers are plausibly related.

APPENDIX A: THE OPTICAL SPECTRUM OF H1419+480

H1419+480 was observed in the 4.2m William Herschel Telescope at the Observatorio del Roque de Los Muchachos in the island of La Palma (Canary Islands, Spain), on February 26, 1998. We used the ISIS double spectrograph with 600 line/mm gratings on both the blue and red arms, with the wavelengths centered at 5200 and 7000 Å respectively, in order to observe the H β +[OIII] region in the blue and the H α + [NII]+[SII] in the red. Weather conditions were good and probably photometric, but the seeing was around 1.5 arcsec. Two 300 sec observations (co-added in the reduction process) were carried out with the slit aligned to parallactic angle. For details on the reduction process, see Barcons et al (2003) as the same setup and procedure was used.

Fig. 12 shows the optical blue and red spectrum of H1419+480. The [OIII] lines have some structure, with two peaks separated $\sim 60 \text{ km s}^{-1}$. This is the main limiting factor in the precision of the redshift, that we measure by fitting both lines to a common redshift and find $z = 0.072296 \pm 0.000004$.

ACKNOWLEDGEMENTS

The work reported herein is based partly on observations obtained with *XMM-Newton*, an ESA science mission with instruments and contributions directly funded by ESA member states and the USA (NASA). It is also based on INES data from the *IUE* observatory. We thank Enrique Solano for assistance with the INES data and an anonymous referee for important suggestions. The *WHT* telescope is operated by the Isaac Newton Group on the Spanish Observatorio del Roque de los Muchachos of the Instituto de Astrofísica de Canarias. We acknowledge financial support by the Ministerio de Ciencia y Tecnología (Spain), under grants AYA2000-1690 and ESP2001-4537-PE.

REFERENCES

- Arnaud K.A., 1996, In ASP Conference Series, Vol 101, 17
- Barcons X., Carrera F.J., Ceballos M.T., 2003, MNRAS, 339, 757
- Blustin A.J., Branduardi-Raymont G., Behar E., Kaastra J.S., Kahn S.M., Page M.J., Sako M., Steenbrugge K.C., 2002, A&A, 392, 453
- Ceballos M.T., Barcons X., 1996, MNRAS, 282, 493
- Crenshaw D.M., Kraemer S.B., Bogges A., Maran S.P., Mushotzky R.F., Wu C.-C., 1999, ApJ, 516, 750
- den Herder J.W., et al., 2001, A&A, 365, L7
- Fabian A.C. et al , 1994, PASJ, 46, L59
- George I.M., Turner T.J., Netzer H., Nandra K., Mushotzky R.F., Yaqoob T., 1998, ApJS, 114, 73
- Halpern J.P., 1984, ApJ, 281, 90

Jansen F.A., et al., 2001, *A&A*, 365, L1
Kinkhabwala A., Behar E., Sako M., Gu M.F., Kahn S.M.,
Paerels F.B.S., 2003, *ApJ*, submitted (astro-ph/0304332)
Lee J.C., Ogle P.M., Canizares C.R., Marshall H.L., Schulz
N.S., Morales R., Fabian A.C., Iwasawa K., 2001, 554, L13
Mason K.O., et al., 2001, *A&A*, 365, L36
Mathur S., 1994, *ApJ*, 431, L75
Mathur S., Wilkes B., Elvis M., Fiore F., 1994, 434, 493
Mathur S., Elvis M., Wilkes B., 1995, *ApJ*, 452, 230
Nandra K., Pounds K.A., 1992, *Nat*, 359, 21
Nandra K., Pounds K.A., 1994, *MNRAS*, 268, 405
Otani C., et al., 1996, *PASJ*, 48, 211
Remillard R., Bradt H.V.D., Brissenden R.J.V., Buckley
D.A.H., Roberts W., Schwartz D.A., Stroozas B.A., Tuohy
I.R., 1993, *AJ*, 105, 2079
Reynolds C.S., Fabian A.C., 1995, *MNRAS*, 273, 1167
Reynolds C.S., 1997, *MNRAS*, 286, 513
Sako M., et al., 2001, *A&A*, 365, L173
Schwope A., et al., 2000, *AN*, 321, 1
Strüder L., et al., 2001, *A&A*, 365, L18
Turner M.J.L. et al., 2001, *A&A*, 365, L27
Whiting E.E., 1968, *J. Quant. Spectrosc. Rad. Transf.*, 8,
1379
Wood K.S., et al., 1984, *ApJS*, 56, 507

This paper has been typeset from a $\text{\TeX}/\text{\LaTeX}$ file prepared
by the author.